Polarization effects on oceanographic lidar

James H. Churnside

NOAA Earth System Research Laboratory
325 Broadway, Boulder, CO 80305
james.h.churnside@noaa.gov

Abstract: A simplified radiative transfer equation yields a simple analytic expression for the co- and cross-polarized return in a linearly polarized oceanographic lidar. This equation agrees well with the lidar data over a wide range of oceanographic conditions. The relationship between depolarization and lidar attenuation shows three distinct relationships corresponding to water within the Columbia River plume, near-shore water outside of the plume, and off-shore water.

OCIS codes: (010.0010) Atmospheric and oceanic optics; (010.3640) Lidar; (010.4450) Oceanic optics; (010.4455) Oceanic propagation; (010.4458) Oceanic scattering; (010.5620) Radiative transfer

References and links

1. B. Billard, R. H. Abbot, and M. F. Penny, "Airborne estimation of sea turbidity parameters from the WRELADS laser airborne depth sounder, "Appl. Opt. **25**, 2080-2088 (1986).
2. F. E. Hoge, C. W. Wright, W. B. Krabill, R. R. Buntzen, G. D. Gilbert, R. N. Swift, J. K. Yungel, and R. E. Berry, Airborne lidar detection of subsurface oceanic scattering layers," Appl. Opt. **27**, 3969-3977 (1988).
3. J. H. Churnside, J. J. Wilson, and V. V. Tatarskii, "Lidar profiles of fish schools," Appl. Opt. **36**, 6011-6020 (1997).
4. J. H. Churnside and R. E. Thorne, "Comparison of airborne lidar measurements with 420 kHz echo-sounder measurements of zooplankton," Appl. Opt. **44**, 5504-5511 (2005).
5. J. H. Churnside and L. A. Ostrovsky, "Lidar observation of a strongly nonlinear internal wave train in the Gulf of Alaska," Int. J. Remote Sens. **26**, 167-177 (2005).
6. G. M. Krekov, M. M. Krekova, and V. S. Shamanaev, "Laser sensing of a subsurface oceanic layer. II. Polarization characteristics of signals," Appl. Opt. **37**, 1596-1601 (1998).
7. A. P. Vasilkov, Y. A. Goldin, B. A. Gureev, F. E. Hoge, R. N. Swift, and C. W. Wright, "Airborne polarized lidar detection of scattering layers in the ocean," Appl. Opt. **40**, 4353-4364 (2001).
8. J. L. Squire and H. Krumboltz, "Profiling pelagic fish schools using airborne optical lasers and other remote sensing techniques," Marine Tech. Soc. J. **15**, 27-31 (1981).
9. J. H. Churnside, K Sawada, and T. Okumura, "A Comparison of Airborne Lidar and Echo Sounder Performance in Fisheries," J. Marine Acoust. Soc. Jpn. **28**, 49-61 (2001)
10. J. H. Churnside, D. A. Demer, and B. Mahmoudi, "A Comparison of Lidar and Echosounder Measurements of Fish Schools in the Gulf of Mexico," ICES J. Mar. Sci. **60**, 147–154 (2003).
11. P. Carrera, J. H. Churnside, G. Boyra, V. Marques, C. Scalabrin and A. Uriarte, "Comparison of airborne lidar with echosounders: a case study in the coastal Atlantic waters of southern Europe," ICES J. Mar. Sci. **63**, 1736-1750 (2006).
12. H. R. Gordon, "Effects of airborne oceanic lidar: effects of multiple scattering," Appl. Opt. **21**, 2996-3001 (1982).
13. D. M. Phillips, R. H. Abbot, and M. F. Penny, "Remote sensing of sea water turbidity with an airborne laser system, J. Phys. D: Appl. Phys. **17**, 1749-1758 (1984).
14. A. P. Vasilkov, T. V. Kondranin, and Ye. V. Myasnikov, "Determining the profile for the light scattering coefficient based on the polarization properties of back-reflected radiation during pulsed sounding of the ocean," Izv., Atmos. Oceanic Phys. **26**, 224-228 (1990).
15. A. P. Vasilkov, Y. A. Goldin, and B. A. Gureev, "Airborne lidar polarization estimation of the vertical profile of seawater light scattering coefficient," Izv. Atmos. Oceanic Phys. **33**, 519-524 (1997).
16. H. H. Kim, "New algae mapping technique by the use of an airborne laser flourosensor," Appl. Opt. **12**, 1454-1459 (1973).
17. F. E. Hoge and R. N. Swift, "Airborne dual-laser excitation and mapping of phytoplankton pigments in a gulf stream warm core ring," Appl. Opt. **22**, 2272-2281 (1983).

#90418 - $15.00 USD Received 3 Dec 2007; revised 8 Jan 2008; accepted 10 Jan 2008; published 16 Jan 2008

18. F. E. Hoge, P. E. Lyon, C. W. Wright, R. N. Swift, and J. K. Yungel, "Chlorophyll biomass in the global oceans: airborne lidar retrieval using fluorescence of both chlorophyll and chromophoric dissolved organic matter," Appl. Opt. **44**, 2857-2862 (2005).
19. E. P. Zege and L. I. Chaykovskaya, "Approximate equations of polarized radiation transport in media with strongly anisotropic scattering," Izv. Atmos. Oceanic Phys. **21**, 796-800 (1985).
20. M. J. Raković and G. W. Kattawar, "Theoretical analysis of polarization patterns from incoherent backscattering of light," Appl. Opt. **37**, 3333-3338 (1998).
21. M. J. Raković, G. W. Kattawar, M. Mehrűbeoğlu, B. D. Cameron, L. V. Wang, S. Rastegar, and G. L. Cote, "Light backscattering polarization patterns from turbid media: theory and experiment," Appl. Opt. **38**, 3399-3408 (1999).
22. K. Mitra and J. H. Churnside, "Transient radiative transfer equation applied oceanographic lidar," Appl. Opt. **38**, 889-895 (1999).
23. K. J. Voss and E. S. Fry, "Measurement of the Mueller matrix for ocean water," Appl. Opt. **23**, 4427-4439 (1984).
24. C. Cox and W. Munk, "Statistics of the sea surface derived from sun glitter," J. Mar. Res. **13,** 198–227 (1954).
25. C. Cox and W. Munk, "Measurement of the roughness of the sea surface from photographs of the sun's glitter," J. Opt. Soc. Am. **44**, 838–850 (1954).
26. J. A. Shaw and J. H. Churnside, "Scanning-Laser Glint Measurements of Sea-Surface Slope Statistics," Appl. Opt. **36**, 4202-4213 (1997).
27. H. R. Gordon, "Simple calculation of the diffuse reflectance of the ocean," Appl. Opt. **12**, 2803-2804 (1973).
28. A. Ben-David, "Mueller matrices and information derived from linear polarization lidar measurements: theory," Appl. Opt. **37**, 2448-2463 (1998).
29. H. M. Zorn, J. H. Churnside, and C. W. Oliver, "Laser safety thresholds for Cetaceans and Pinnipeds," Marine Mammal Sci. **16**, 186-200 (2000).
30. R. C. Smith and K. S. Baker, "Optical properties of the clearest natural waters (200-800 nm)," Appl. Opt. **20**, 177-184 (1981).
31. A. P. Vasilkov, T. V. Kondranin, and Ye. V. Myasnikov, "Polarization characteristics in the backscattering signal for pulsed sensing of the ocean by a narrow light beam," Izv., Atmos. Oceanic Phys. **24**, 635-642 (1988).

1. Introduction

There are few options available to those who would probe the ocean from above the surface. Of these, only lidar operating in the blue-green region of the spectrum is capable of producing vertical profiles to a few tens of meters with sub-meter resolution. Despite this, there are only a few lidars that have been used to profile the ocean, at least in part because of the difficulties in interpreting the lidar return signal.

Scattering layers in the ocean are detectable by an unpolarized lidar [1,2]. Through the use of a cross-polarized lidar, the contrast between scattering layers and the background scattering level can be increased for a scattering layer comprising large, depolarizing particles [3]. This type of lidar has been used effectively to detect plankton layers [4,5]. A fully polarized lidar is expected to provide even better discrimination of scattering layers [6,7].

Of course, a fish school is a special case of a scattering layer with different polarization characteristics from those of the surrounding water. Lidar detection of a fish school was first reported in 1981 [8]. More recent work has shown good agreement between lidar and more traditional acoustic techniques of detecting and quantifying fish schools [9-11].

There have also been several efforts to infer the optical properties of the water from lidar signals. Gordon [12] showed how an unpolarized lidar could be used to measure either the beam attenuation coefficient with a narrow beam or the diffuse attenuation coefficient with a broad beam. Phillips, et al. [13] and Billard, et al. [1] measured various parameters related to turbidity. Vasilkov and co-workers [7,14,15] used a polarized lidar to infer the scattering coefficient profile.

A slightly different type of oceanographic lidar uses a laser to stimulate fluorescence of organic molecules in the water. This was first used to detect chlorophyll *a* [16]. Phycoerythrin and chromophoric dissolved organic matter (CDOM) have also been measured [17,18]. Fluorescence is unpolarized for any polarization of the stimulating light, so the results presented here do not apply to fluorescence lidar measurements.

#90418 - $15.00 USD Received 3 Dec 2007; revised 8 Jan 2008; accepted 10 Jan 2008; published 16 Jan 2008

Much of the previous work has focused on the detection of scattering layers in the ocean. We will focus on regions where the scattering properties are constant with depth over the depth range accessible to the lidar. Also, much of the previous work has considered a narrow lidar beam [7]. We will consider the case of a broader beam, so that multiple scattering plays a greater role [12]. Here, we show that the depolarization induced by multiple forward scattering can be distinguished from that induced by backscattering, so the depolarization characteristics of the lidar target can be accurately estimated.

2. Theory

The theoretical treatment is based on a simplified version of the radiative transfer equation for the Stoke's vector [19]. The main simplification arises because we are only interested in the direct backscattered light, and not in the full radiance distribution treated by others [20, 21]. Also, we will not treat temporal effects explicitly as in [22], but relate the time of the return signal to depth through the speed of light in water. We assume a linearly polarized transmitter, and consider only light that is co-polarized with the transmitted light or cross-polarized with respect to it. The primary justification for this simplification is that the off-diagonal elements of the Mueller matrix for scattering by sea water are negligible, except for M_{12} and M_{21}, which relate the two orthogonal linear polarizations [23].

As the initially polarized laser beam propagates through sea water, the change in the power of the beam can be expressed as

$$\begin{aligned} \frac{dP_C}{dz} &= -\alpha P_C + \gamma P_X \\ \frac{dP_X}{dz} &= -\alpha P_X + \gamma P_C \,, \end{aligned} \tag{1}$$

where P_C is the power at depth z in the initial linear polarization, P_X is the power in the orthogonal polarization, α is the attenuation of a polarized beam, and γ is the depolarization coefficient. The depolarization coefficient represents the rate at which light from one polarization is scattered into the other.

For a linearly polarized lidar transmitter, the boundary conditions at $z = 0$ are $P_X = 0$ and $P_C = P_{C0}$, where P_{C0} is the initial power. This leads to the solution

$$\begin{aligned} P_C &= P_{C0} \exp(-\alpha z) \cosh(\gamma z) \\ P_X &= P_{C0} \exp(-\alpha z) \sinh(\gamma z) . \end{aligned} \tag{2}$$

For $\gamma z << 1$, this reduces to

$$\begin{aligned} P_C &= P_{C0} \exp(-\alpha z) \\ P_X &= P_{C0} \gamma z \exp(-\alpha z) . \end{aligned} \tag{3}$$

For the opposite case of $\gamma z >> 1$, Eq. (2) reduces to

$$P_C = P_X = 0.5 P_{C0} \exp(-\alpha z + \gamma z) . \tag{4}$$

The last Eq. (4) also holds if the initial light is unpolarized, so the attenuation coefficient of an unpolarized lidar is $\alpha - \gamma$.

Figure 1 shows the theoretical profiles of power in the water for the case of $\gamma = 0.1\alpha$. The maximum value of the cross-polarized power is at a depth of α^{-1}. The mostly-polarized approximation [Eq. (3)] is seen to better explain the cross-polarized component than the co-polarized component. For example, the approximation is good to within about 10% to a

#90418 - $15.00 USD Received 3 Dec 2007; revised 8 Jan 2008; accepted 10 Jan 2008; published 16 Jan 2008

depth of about $5\alpha^{-1}$ ($\gamma z = 0.5$) for the co-polarized component, but to a depth of about $8\alpha^{-1}$ ($\gamma z = 0.8$) for the cross-polarized component. The unpolarized approximation [Eq. (4)] is within 20% for both components by the time we reach a depth $z = 10\alpha^{-1}$ ($\gamma z = 1$).

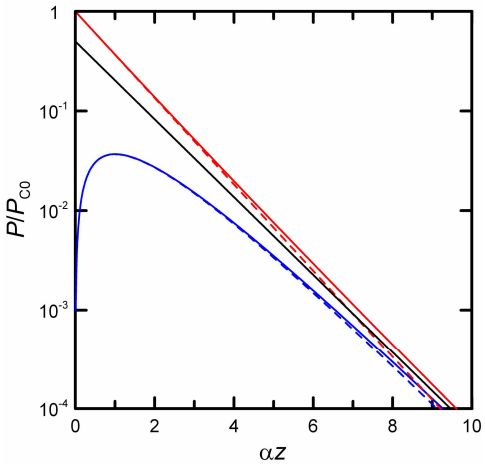

Fig. 1. Laser power P normalized to incident power P_{C0} for co-polarized (red) and cross-polarized (blue) components for the case of $\gamma = 0.1\alpha$. Solid lines are the exact calculation, dashed lines are the mostly-polarized approximation, black line is the unpolarized approximation.

In Eq. (2), we have neglected depolarization because of Fresnel transmission differences at the surface. To get an estimate of the magnitude of depolarization by the rough surface, we assumed a Gaussian probability density of surface slopes. The slope variance in the along-wind and cross-wind directions were obtained from [24, 25],

$$\begin{aligned} \sigma_U^2 &= 0.00316\, W \\ \sigma_V^2 &= 0.00192\, W + 0.003\,, \end{aligned} \tag{5}$$

where W is the wind speed. These formulae neglect the effects of surfactants [24, 25] and atmospheric stability [26]. The resulting depolarization (Fig. 2) is small, even when the lidar is pointed slightly off nadir to reduce specular reflections from the surface.

In the quasi-single-scattering approximation [14,27], we assume that the light propagates through the water with a series of scattering events at small scattering angles, undergoes a backscattering event, and then propagates back to the surface with only small-angle scattering events. If the depolarization is small, the co-polarized signal (S_C) from the lidar can be approximated by neglecting the depolarized light, so

$$S_C(t) = A' P_C \beta_C(\pi) \exp(-\alpha z) \quad , \tag{6}$$

where A' includes system parameters like receiver sensitivity, $\beta_C(\pi)$ is the polarization-preserving component of the volume scattering coefficient at a scattering angle of π, and $\exp(-\alpha z)$ is the attenuation of the backscattered light as it propagates up to the surface. The time t is the time at which the lidar signal would have been backscattered from depth z based on the speed of light in water; this allows a vertical profile to be inferred from a temporal measurement at the receiver.

#90418 - $15.00 USD Received 3 Dec 2007; revised 8 Jan 2008; accepted 10 Jan 2008; published 16 Jan 2008

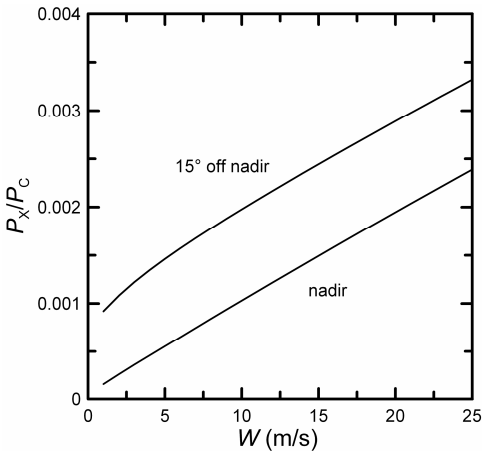

Fig. 2. Depolarization of a linearly polarized laser beam propagating through the sea surface as a function of wind speed W. The two curves are for a nadir-pointing beam and for one pointed 15° off nadir.

The cross-polarized signal (S_X) is the sum of three components; in one, the depolarization is caused by the backscattering event and, in the other two, the depolarization is caused by the multiple forward scattering before and after the backscattering event, respectively. Thus,

$$S_X(t) = A' P_C \beta_X(\pi) \exp(-\alpha z) + A' P_X \beta_C(\pi) \exp(-\alpha z) + A' P_C \beta_C(\pi) \gamma z \exp(-\alpha z), \quad (7)$$

where $\beta_X(\pi)$ is the cross-polarizing component of the volume scattering. The use of the same system parameter A' in Eqs. (6) and (7) implies that this parameter is the same for the co- and cross-polarized channels of the lidar receiver. In the description of the measurements, we will define the lidar signals S_C and S_X so that this is the case.

Using Eq. (3) in Eqs. (6) and (7), and replacing $A' P_{C0}$ by A yields the result

$$\begin{aligned} S_C(t) &= A \beta_C(\pi) \exp(-2\alpha z) \\ S_X(t) &= A \beta_X(\pi) \exp(-2\alpha z) + 2A \beta_C(\pi) \gamma z \exp(-2\alpha z). \end{aligned} \quad (8)$$

The depolarization ratio of the lidar return is then given by

$$D = \frac{S_X}{S_C} = \frac{\beta_X(\pi)}{\beta_C(\pi)} + 2\gamma z. \quad (9)$$

3. Measurements

The measurements were made with the NOAA Fish Lidar flying at an altitude of about 300 m off the west coast of Oregon and Washington. We will use the results from a flight made between about 22:00 local time on June 10 and 1:00 on June 11, 2006, along the line shown in Fig. 3. The constant-latitude transects are about 350 km long. The lidar has been described in previous publications [3-5], except that a second polarization channel has been added. It uses a tristatic configuration, with separated transmitter, co-polarized receiver, and cross-polarized receiver.

The transmitter uses a frequency-doubled, Q-switched Nd:YAG laser. It produces 120 mJ of green (532 nm) light in a 12 ns pulse at a rate of 30 pulses per second. A polarizing beamsplitter in front of the laser increases the polarization purity of the transmitted light to greater than 0.999, and also provides a small signal to a detector for a timing reference. A

#90418 - $15.00 USD Received 3 Dec 2007; revised 8 Jan 2008; accepted 10 Jan 2008; published 16 Jan 2008

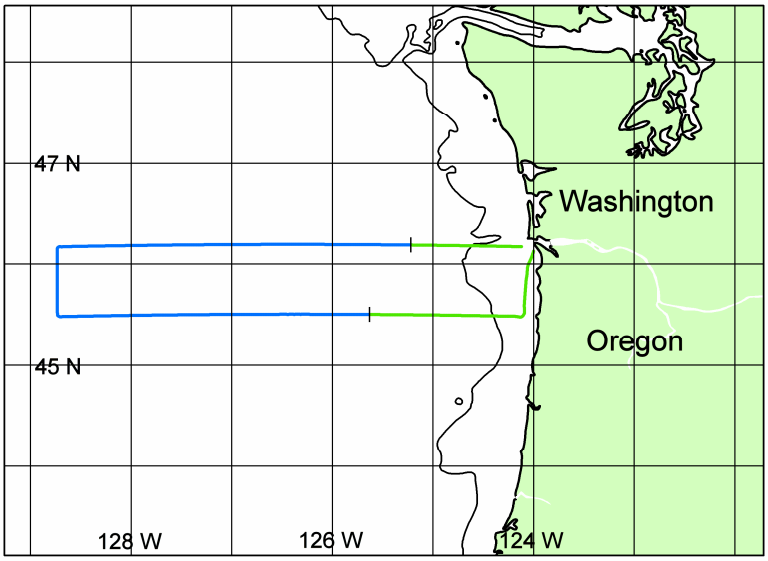

Fig. 3. Position of measurements showing the near-shore (green) and off-shore (blue) segments, with a vertical mark at the boundary. The solid black line is the 200 m isobath. The mouth of the Columbia River is just to the east of the northern transect.

pair of steering mirrors in front of the beamsplitter is used for alignment. The final optical element is a negative lens that spreads the beam to about 17 mrad. This produces a 5 m diameter spot on the sea surface, which is safe for people or marine mammals [28] at the surface.

Each receiver channel uses a refractive telescope with a Polaroid filter on the front. The primary lens focuses the light onto an aperture that restricts the field of view to about 17 mrad. A secondary lens recollimates the light, and it passes through a 1 nm bandwidth interference filter and is detected by a photomultiplier tube. Because there is more reflected light in the co-polarized channel than the cross-polarized channel, the diameters of the two telescopes are different – roughly 6 cm and 15 cm, respectively.

The photomultiplier outputs are logarithmically amplified and digitized at 1 GHz. The digitized data are stored in the computer, along with the position and time of each pulse from the GPS receiver. The gain-control voltages applied to the photomultipliers are also recorded, since the gains are adjusted to accommodate different signal levels from different areas of the ocean.

While the obvious definition of the lidar signals S_C and S_X would be the voltages out of the receiver, some manipulation of these voltages produces signals that are more convenient to compare with the theoretical results. First, the recorded voltages are converted to the corresponding photocathode current, using the measured response of the log-amplifiers and the recorded photomultiplier gains. This provides a linear response that is the same at every location. Then, these values were normalized by the measured sensitivities of the co- and cross-polarized receivers. This step accounts for the different telescope diameters, optical losses, and photocathode responsivities, so that the system parameter A is the same for both channels. Finally, these values were corrected for the change in the geometric, or range squared, signal loss with depth. This effect is relatively small – a difference of about 15% at a depth of 30 m with an aircraft altitude of 300 m. The correction was made because the geometric loss was neglected in the development of Eq. (8). The results of these three steps define our lidar signals S_C and S_X.

#90418 - $15.00 USD Received 3 Dec 2007; revised 8 Jan 2008; accepted 10 Jan 2008; published 16 Jan 2008

During the period of the flight, the average wind at 124.51 W, 46.14 N (NOAA buoy 46029) was 7.2 m s^{-1} from 350˚. For these conditions, we would expect the standard deviation of surface tilt to be about 8.6˚ in the N-S direction and about 7.4˚ in the E-W direction. Thus, the surface depolarization was less than 0.002, and can be neglected.

In regions where the water properties are constant with depth, we can estimate the model parameters from the theoretical results. We can estimate α from the measured co-polarized signal using the first of Eq. (8), with the result

$$\alpha = -\tfrac{1}{2}\frac{d}{dz}\ln(S_C). \tag{10}$$

Similarly, we can estimate γ from the measured depolarization using Eq. (9) with the result

$$\gamma = \tfrac{1}{2}\frac{dD}{dz}. \tag{11}$$

4. Results

We will first consider a couple of typical profiles to illustrate the characteristics of the lidar return. The first (Fig. 4, left panel) was obtained in shallow water near the coast. The return from aerosols above the surface is visible in the co-polarized return, but below the receiver noise level in the cross-polarized return; the backscatter from small, nearly spherical marine aerosols is highly polarized. The co-polarized return has an enhancement at the surface from laser glints; this specular reflection is also highly polarized. This profile also includes the return from the bottom at a depth of about 22 m. The return from the rough bottom is completely depolarized, and the two channels have the same signal level.

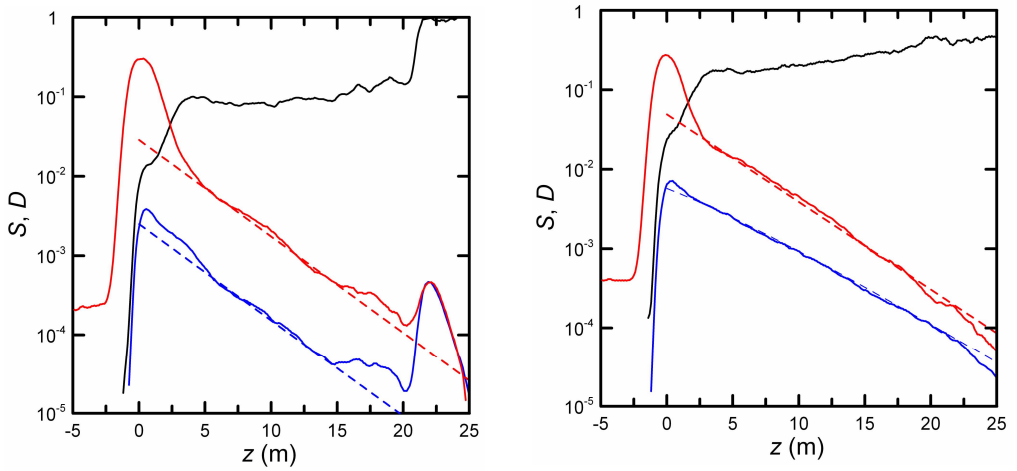

Fig.4. Typical depth profiles of the co-polarized return S_C (red), cross-polarized return S_X (blue), and depolarization D (black). The solid lines are measured values, and the dashed lines are the theoretical profiles from Eq. (8). The left panel is from the near-shore region. The large, unpolarized return at 22 m depth is the bottom of the ocean. The right panel is from the off-shore region.

Between the surface return and the bottom, both channels attenuate at about the same rate, with a nearly constant depolarization of about 0.0873 (average between 5 and 15 m). The co-polarized return can be approximated by Eq. (8), with the parameters taken from the values at 5 and 15 m. This gives α = 0.140 m^{-1} and $A\beta_C(\pi)$ = 0.0287. This provides a good approximation to the measured profile, except for a layer of enhanced scattering near the

#90418 - $15.00 USD Received 3 Dec 2007; revised 8 Jan 2008; accepted 10 Jan 2008; published 16 Jan 2008

bottom. From Eq. (9), it is clear that the nearly constant depolarization ratio means that γ is very close to 0. Thus, the cross-polarized return is given by Eq. (8) with $A\beta_X(\pi) = 2.51\times10^{-3}$.

The second profile (Fig. 4, right panel) was obtained farther from the coast. Here, the attenuation of the two channels is different, and the depolarization increases with depth. From the co-polarized return at 5 m and 15 m, we estimate the parameters of Eq. (8) to be α = 0.127 m^{-1} and $A\beta_C(\pi)$ = 0.0492, which implies that there is less attenuation and more backscatter than observed near the coast. A linear regression of the depolarization values between 6 and 16 m produces an estimate of $\gamma = 6.12\times10^{-3}$ m^{-1}. The cross-polarized return at 12 m depth was used to estimate the final parameter in Eq. (8), with the result that $A\beta_X(\pi)$ = 5.73×10^{-3}. The depolarization induced by scattering for this case is 0.116, which is greater than that near the coast. The results in the right panel also show a good agreement between the theoretical and observed returns. The fit is actually better than that near the coast; the most likely explanation is that the upper water column is more uniform off shore than in the river plume.

To investigate how the propagation parameters vary with changes in the water column, we looked at the co- and cross-polarized returns over the depth range between 5 and 10 m, and averaged over about 5 km along the flight track. Figure 5 is a plot of α as a function of longitude along the northern and southern east-west transects. The observed values were generally around 0.1 in the off-shore regions and higher closer to shore. This plot shows that the higher values extend farther to the west in the southern transect. This is consistent with the position of the Columbia River plume, which extended to the southwest from the mouth of the river. In the southern transect, α has a peak at about 124˚ W, suggesting that the center of the plume is at about this position. The eastern-most longitude at which α passed through 0.1 m^{-1} in each transect was used to divide the data into the off-shore and near-shore segments shown in Fig. 3.

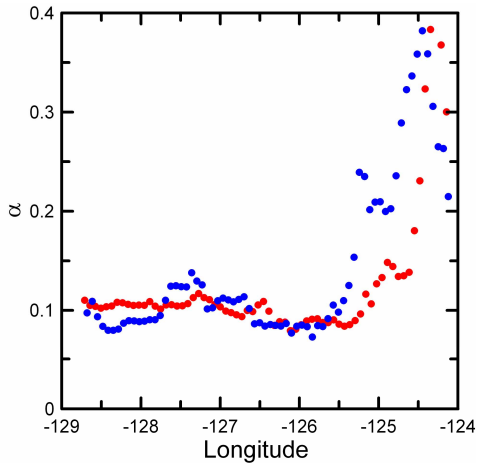

Fig. 5. Measured values of attenuation coefficient α as a function of longitude for the northern (red) and southern (blue) east-west transects.

The cross-polarized returns in Fig. 4 appear to be nearly exponential. Thus, it makes sense to compare the measured attenuation of the cross-polarized signal with the derivative of the logarithm of Eq. (8). The result was that 99% of the values were within 3% of the value inferred from Eq. (8), and 89% were within 1%. This agreement suggests that our simple model is a useful one.

#90418 - $15.00 USD Received 3 Dec 2007; revised 8 Jan 2008; accepted 10 Jan 2008; published 16 Jan 2008

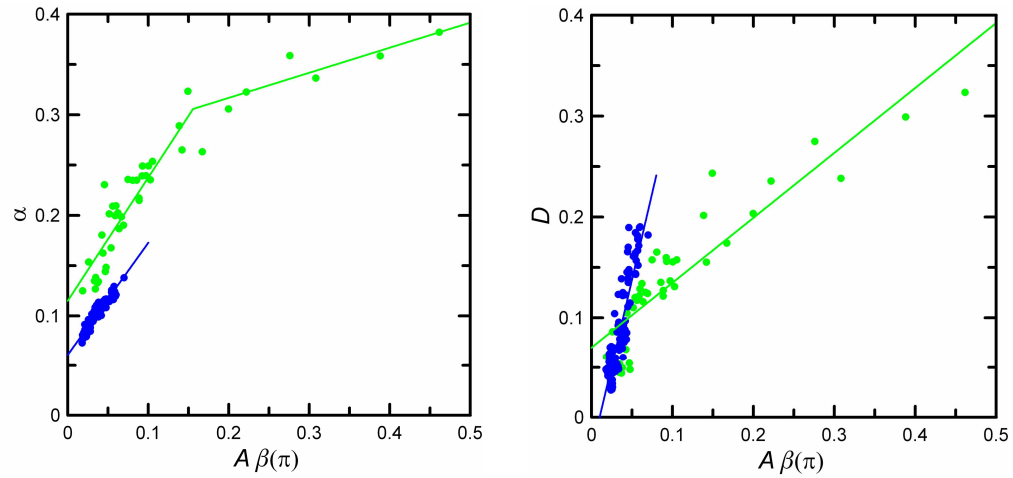

Fig. 6. Total attenuation α (left panel) and depolarization D (right panel) as functions of backscatter. The blue circles and line are the off-shore data and linear regression. The green circles and lines are the near-shore data and a piecewise linear regression.

We found an interesting relationship between α and the total backscatter, $\beta(\pi) = \beta_C(\pi) + \beta_X(\pi)$ (Fig. 6, left panel). For the off-shore region, the attenuation is very nearly linear with respect to backscatter; the regression ($R^2 = 0.92$) is

$$\alpha = 1.11A\beta(\pi) + 0.0612 . \quad (11)$$

For the near-shore region, there is not a single linear relationship, but the data can be described by two different regression curves with a break where $\alpha = 0.3$ m^{-1}. For the lower values, the regression ($R^2 = 0.80$) is

$$\alpha = 1.23A\beta(\pi) + 0.115 . \quad (12)$$

For the higher values, the regression ($R^2 = 0.81$) is

$$\alpha = 0.249A\beta(\pi) + 0.267 . \quad (13)$$

Equation (13) generally describes water that we associate with the Columbia River plume. The large y-intercept suggests high levels of dissolved absorbing materials. Equation (12) generally describes coastal water outside of the plume, which has a y-intercept between the open-ocean value in Eq. (11) and the river plume value in Eq. (13).

If we plot the depolarization, averaged over the depth range between 5 and 10 m, as a function of the total backscatter (Fig. 6, right panel), we find a high correlation for both near-shore ($R^2 = 0.81$) and off-shore ($R^2 = 0.78$) data. At the lower values, the near-shore and off-shore data are very nearly the same. A similar plot of depolarization as a function of attenuation coefficient (Fig. 7, left panel) shows a different pattern. Here, the correlation is very high ($R^2 = 0.95$) in the near-shore region, but not as high ($R^2 = 0.66$) off shore.

For the near-shore region, we found that γ varied randomly about zero. The average value was -1.43×10^{-3} m^{-1}, and the standard deviation of the 42 observations was 3.92×10^{-3} m^{-1}. There was no significant correlation ($R^2 = 0.11$) between α and γ in this region. For the off-shore region, the situation is different; γ is significantly different from 0 and increases with increasing backscatter ($R^2 = 0.73$) (Fig. 7, right panel).

#90418 - $15.00 USD Received 3 Dec 2007; revised 8 Jan 2008; accepted 10 Jan 2008; published 16 Jan 2008

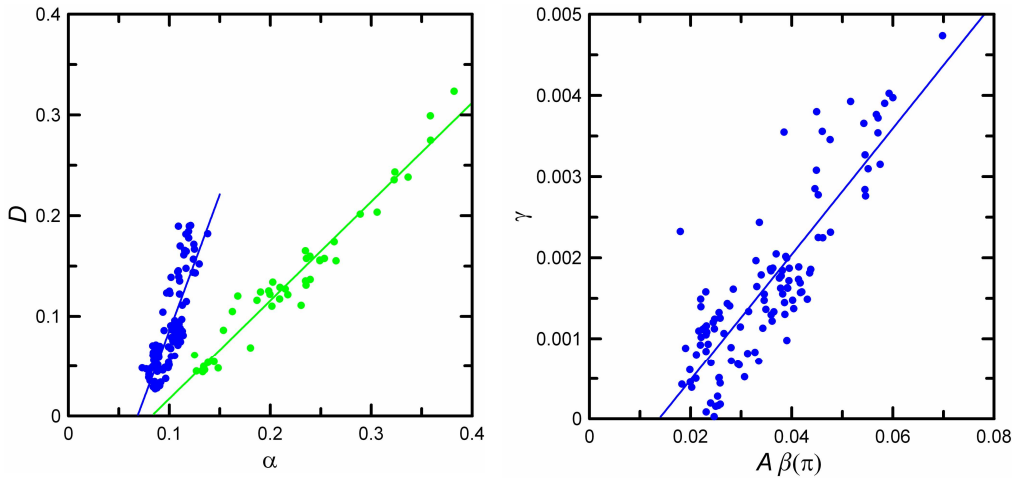

Fig. 7. Depolarization D as a function of attenuation coefficient α (left panel) and depolarization coefficient γ as a function of backscatter (right panel). Green is near-shore region and blue is off-shore region. Points are data and lines are linear regression.

The average values for each region are presented in Table 1, and the theoretical profiles

Table 1. Average parameter values.

Region	$A\,\beta_C(\pi)$	$A\,\beta_X(\pi)$	α	γ	D
N transect	0.0420	0.00276	0.121	1.75×10^{-3}	0.0658
S transect	0.0591	0.00862	0.143	5.81×10^{-4}	0.146
Near shore	0.0964	0.0170	0.224	-1.43×10^{-3}	0.177
Off shore	0.0331	0.00228	0.100	1.64×10^{-3}	0.0690

using these values (with $\gamma = 0$ for the near-shore profiles) are plotted in Fig. 8. These clearly show the different regimes. In the near-shore region the signal level is higher at the surface (more backscattering) but decreases more rapidly (more attenuation).

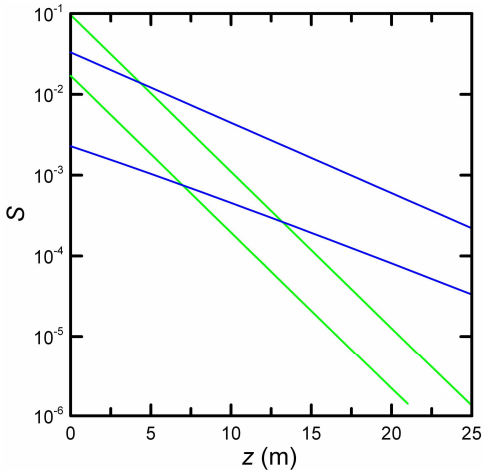

Fig. 8. Depth profiles using the average parameters of Table 1 (with $\gamma = 0$ for the near shore) for the near-shore (green) and off-shore (blue) regions. In each case, the upper curve is the co-polarized return and the lower curve is the cross-polarized return.

#90418 - $15.00 USD Received 3 Dec 2007; revised 8 Jan 2008; accepted 10 Jan 2008; published 16 Jan 2008

6. Discussion

It is tempting to assume that, at least within each of our regions, the optical properties of the scatterers within the water are constant, and changes in the lidar signals are due to variations in number density. Vasilkov, *et al*., [7] use a similar assumption to infer the vertical profiles of scattering coefficient, *b*. Phillips, *et al*., [13] make a similar assumption to infer absorption coefficient, *a*, and *b* from airborne lidar. If this assumption were valid, we would expect a linear relationship between attenuation and total backscatter, since both would depend linearly on the number density of scatterers. That is, $\alpha = a_w + N\sigma_T$, where a_w is the absorption coefficient for water and dissolved substances (not including particulate absorption), N is the number density of particles and σ_T is the average value of the total cross section (absorption and absorption) of a single particle; and $\beta(\pi) = N\sigma_\pi$, where σ_π is the average cross section for backscatter into a unit solid angle of a single particle; so

$$\alpha = a_w + \frac{\sigma_T}{\sigma_\pi}\beta(\pi) . \tag{14}$$

This assumes that the absorption by the water does not depend on N within each of our regions. If, instead, there is a component to the absorption by water that is correlated with particle number density, we would include this in σ_T, rather than in a_w, and misinterpret it as a property of the particles.

If we look at the dependence of attenuation on backscatter (Fig. 6), we do see a linear relationship in each of the water masses we have identified. The slopes for the waters with the lowest backscatter values are very similar for the near-shore (1.225 ± 0.106) and off-shore (1.115 ± 0.031) regions. The difference (0.11 ± 0.11) is within the combined error of the regressions. This suggests that the scattering particles are similar in the regions, and the main difference is a difference in the absorption of the water, which we can estimate by comparing Eq. (14) with Eqs. (11) and (12) to get $a_w = 0.061$ m^{-1} off shore and $a_w = 0.115$ m^{-1} near shore. For reference, the measured absorption of very clear natural seawater at our wavelength is 0.052 m^{-1} [29], so the seawater component dominates in the off-shore region. However, the water that we associate with the Columbia River plume has very different characteristics. The absorption suggested by Eq. (13), $a_w = 0.267$ m^{-1}, is much higher, and the attenuation increases less rapidly with increasing backscatter. This suggests that the characteristics of the scattering particles are different in the plume from those outside of it, although there is another possibility that should be mentioned; there could be variations in water absorption that are correlated with particle density, with different relationships between water absorption and particle density in the plume from those outside. We note that Billard, *et a.,l* [1] have also identified different water masses with different relationships between attenuation and backscatter, and differences in particle characteristics are the more likely explanation.

If the optical properties of the scatterers within the water are constant, we would further expect that the depolarization, after correcting for the effects of multiple scattering, would be constant. However, our depolarization data do not support the assumption that the properties of the scatterers are constant. Instead, we see a linear relationship between depolarization and backscatter (Fig. 6). Equation (9) shows that multiple scattering does not explain this relationship. We conclude that higher backscatter levels must be associated with particles that are more depolarizing. This would suggest more irregularly shaped scatterers that are larger and/or have a greater refractive index. This applies, of course, to the collection of particles within the scattering volume; we cannot associate the depolarization of the return with that from a single particle, because the co-polarized return might be dominated by small, spherical particles and the cross-polarized return from large, irregular particles.

Vasilkov, *et al*., [30] found that the depolarization caused by multiple scattering should depend on the single-scattering albedo; if the single-scattering albedo is low, there is not as

#90418 - $15.00 USD Received 3 Dec 2007; revised 8 Jan 2008; accepted 10 Jan 2008; published 16 Jan 2008

much multiple scattering. Our data support this – γ is essentially zero in the near-shore region where the absorption is high.

The conclusion is that the simplified radiative transfer equations accurately describe the return from polarized lidar in the ocean. These results justify the exponential approximation to the decay of the co-polarized return with depth. They suggest how the depolarization caused by multiple forward scattering might be distinguished from the depolarization caused by backscattering. These results also help understand the different optical properties of different water masses.

Acknowledgments

This work was supported by the National Ocean Partnership Program and the NOAA Office of Ocean Exploration. The general solution of Eq. (2) was pointed out by one of the reviewers.

#90418 - $15.00 USD Received 3 Dec 2007; revised 8 Jan 2008; accepted 10 Jan 2008; published 16 Jan 2008